Localization and advectional spreading of convective flows under parametric disorder

Denis S. Goldobin[1,2] and Elizaveta V. Shklyaeva[1]

[1] *Department of Theoretical Physics, Perm State University, 15 Bukireva str., 614990, Perm, Russia*
[2] *Department of Physics and Astronomy, University of Potsdam, Postfach 601553, D–14415 Potsdam, Germany*

We study thermal convection in a thin horizontal porous layer heated from below in the presence of a parametric disorder. Parameters are time-independent, but inhomogeneous in one of the horizontal directions. Under frozen parametric disorder, spatially localized flow patterns appear. We focus our study on their localization properties and the effect of an imposed longitudinal advection on these properties. Our interpretation of the results of the linear theory is underpinned by a numerical simulation for the nonlinear problem. For weak advection leading to upstream delocalization, the transition from a set of localized flow patches to an almost everywhere intense "global" flow occurs moderately below the instability threshold of the disorderless system. Strong advection leads to a washing-out of the localized flows and possible scenarios of this washing-out are discussed. The results presented are relevant for a broad variety of active media where pattern selection occurs.

PACS numbers: 05.40.-a, 44.25.+f, 47.54.-r, 72.15.Rn

I. INTRODUCTION

The interest to the effect of localization in spatially extended systems under parametric disorder was first initiated in the context of phenomena in quantum systems; this effect, Anderson localization [1] (AL), has been originally discussed for such processes as spin diffusion or electron propagation in a disordered potential. Later on, AL was studied in various branches of physics in the context of waves propagation in randomly inhomogeneous acoustic ([2] and refs. therein), optical media (*e.g.*, [3] and refs. therein), *etc.* AL occurs not only for a random parametric inhomogeneity but also for a quasi-periodic one (*e.g.*, [4, 5, 6]). The common point for the listed works is that they deal with conservative media (or systems) in contrast to active/dissipative ones like in the problems of thermal convection.

In [7] the effect of parametric disorder on the excitation threshold in an active medium, 1D Ginzburg–Landau equation has been discussed, but the localization effects were beyond the study scope. Noteworthy, the localization properties of solutions to the linearized Ginzburg–Landau equation are identical to the one for the Schrödinger equation (where AL was comprehensively discussed; for instance, see [8, 9, 10]), while for large-scale thermal convection it is so only under specific conditions. To the best of the authors' knowledge, localization (or, in an adapted formulation, *excitation of localized modes*) in the presence of a frozen parametric disorder in fluid dynamics problems (*e.g.*, thermal convection) has not been reported in the literature.

The paper is organized as follows. In Sec. II, we introduce the specific physical system we deal with and its mathematical description, and discuss some general aspects of the problem. Sec. III presents the study of properties of the formal localized solutions to the linearized equations, discussion of the effect of an imposed longitudinal advection (pumping) on these properties, and analytical estimations for localization exponents calculated numerically. Then, in Sec. IV, we underpin our results obtained for formal solutions to the linearized problem with numerical simulation of the non-linearized equations. In Sec. V, results on scenarios of the advectional washing-out of localized convective flows complete our discussion of the role of the advection. Sec. VI finishes the paper with conclusions and argumentation in support of general applicability of our results.

II. LARGE-SCALE THERMAL CONVECTION IN A HORIZONTAL LAYER

A. Basic equations

As a specific physical system, we consider a thin porous layer saturated with a fluid. The layer is confined between two impermeable horizontal plates and heated from below (Fig. 1). The coordinate frame is such that the (x, y)-plane is horizontal, $z = 0$ and $z = h$ are the lower and upper boundaries, respectively. The bounding plates are nearly thermally insulating (compared to the layer) what implies a fixed heat flux through the layer boundaries. This flux $Q(x, y)$ is time-independent but inhomogeneous in space;

$$Q(x, y) = Q_{\rm cr}(1 + \varepsilon^2 q(x, y)) \,,$$

here $Q_{\rm cr}$ is the threshold value of the heat flux for the case of spatially uniform heating (above the threshold, convective flows are excited), ε^2 is a characteristic value of local relative deviations of the heat flux from the critical value. For thermal convection in a porous medium the

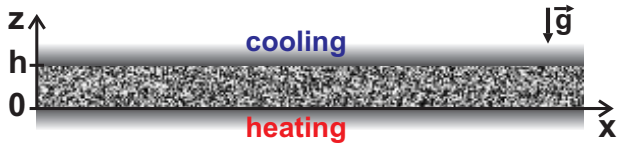

FIG. 1: Sketch of the system and coordinate frame

effects we will discuss appear also when the heating is uniform but the porous matrix is weakly inhomogeneous [11] (this inhomogeneity is inevitable in real systems). Nevertheless, we assume an inhomogeneous heating in order to be able to extend all our results and conclusions to convection without a porous matrix. In this paper, we consider only $q = q(x)$ and the flows homogeneous along the y-direction. Also, we admit a pumping of the fluid along the layer.

For nearly thermally insulating boundaries and a uniform heating, the first convective instability of the layer is long-wavelength [12, 13] (in other words, large-scale), what means that the horizontal scale L of the flow is large against the layer height h; $L = \varepsilon^{-1}h$ [31]. For large-scale convection the temperature perturbations $\theta = \theta(x)$ are almost uniform along z and the system is governed by the dimensionless equation [11]

$$\dot{\theta} = \left(-u\theta - \theta_{xxx} - q(x)\theta_x + (\theta_x)^3\right)_x , \qquad (1)$$

where u is the x-component of the imposed advection (through-flow) velocity. Noteworthy, the same equation governs some other fluid dynamical systems [14, 15, 16]. For Eq. (1) the length scale is set to L and thus the dimensionless layer height $h = \varepsilon \ll 1$.

Though Eq. (1) is valid for a large-scale inhomogeneity, *i.e.*, $h|q_x|/|q| \ll 1$, one may set such a hierarchy of small parameters, namely $\varepsilon \ll (h|q_x|/|q|)^2 \ll 1$, that, on the one hand, the long-wavelength approximation remains valid, whereas, on the other hand, the frozen inhomogeneity may be represented by a δ-correlated Gaussian noise:

$$q(x) = q_0 + \xi(x),\ \langle\xi(x)\rangle = 0,\ \langle\xi(x)\xi(x')\rangle = 2D\delta(x-x'),$$

where q_0 is the mean departure from the instability threshold of the system without disorder (shortly referred as "mean supercriticality"). The noise strength D may be set to 1 by means of the following rescaling: $(x, t, q) \to (D^{-1/3}x, D^{-4/3}t, D^{2/3}q)$ ([32]; henceforth, $D = 1$). As soon as the layer is practically not infinite, one should be subtle with the small noise limit which implies a shrinking of the length of the system owing to the rescaling of the spatial variable.

In specific physical systems described by Eq. (1), properties of various physical fields may differ, and, simultaneously, for particular physical phenomena in these systems, properties of one or another field may play a decisive role. For instance, transport of a pollutant [21] is determined by the velocity field which not necessarily possesses the same localization properties as the temperature field. Therefore, relations between various fields and field θ deserve attention, though all the findings of the paper can be provided in terms of θ regardless to a specific origin of Eq. (1). For a porous layer we consider, the fluid velocity field of the convective flow is

$$\vec{v} = \frac{\partial\Psi}{\partial z}\vec{e}_x - \frac{\partial\Psi}{\partial x}\vec{e}_z , \qquad \Psi = f(z)\,\psi(x,t) , \qquad (2)$$

where $\psi(x,t) \equiv \theta_x(x,t)$ is the stream function amplitude and $f(z) = (3\sqrt{35}/Dh^3)\,z(h-z)$ [11]. The contribution of imposed advection u is not presented here due to its smallness against v ($u \sim 1$ *vs.* $v \sim h^{-2}$). In spite of its smallness, the advection u influences the system dynamics due to its spatial properties; u provides a fluid gross flux through a cross-section of the layer, whereas for the convective flow $\vec{v}$ this gross flux is zero [33]. When the gross flux of a certain flow is zero, the transport (including the heat transfer) by this flow is essentially less efficient compared to the case of a nonzero gross flux. The relationship (2) between the flow and the temperature perturbation is specific for a porous layer and may differ from the ones for other fluid dynamical systems governed by Eq. (1).

B. Excitation of localized modes: general aspects

Numerical simulation reveals only the stable time-independent solutions to establish in the course of the evolution of the dynamical system (1) for small enough u. Hence, the object of our interest are the localization properties of nontrivial time-independent solutions. When some solution is localized near the point x_0, in the distance from x_0,

$$\theta_x \propto \begin{cases} \exp(-\gamma_-|x-x_0|), & (x-x_0)u > 0; \\ \exp(-\gamma_+|x-x_0|), & (x-x_0)u < 0. \end{cases}$$

Here γ_- and γ_+ are the down- and upstream localization exponents, respectively; the inverse value $\lambda_\pm = \gamma_\pm^{-1}$ is called the "localization length". In the region of exponential tails the solutions are small and the exponents may be found from the linearized form of Eq. (1), which can be once integrated in the stationary case;

$$u\theta + \theta''' + [q_0 + \xi(x)]\theta' = const \equiv S \qquad (3)$$

(the prime denotes the x-derivative). For $u \neq 0$ the substitution $\theta \to \theta + S/u$ sets S to zero.

Let us now compare our problem to the Schrödinger equation, a paradigmatic model for AL, and recall some results from the classical theory of AL, which are relevant for our study.

For $u = S = 0$, θ_x is governed by the stationary Schrödinger equation with the mean supercriticality q_0 instead of the state energy and $\xi(x)$ instead of the potential. For the Schrödinger equation with a δ-correlated potential the AL is comprehensively studied; all states (for any energy) are localized (*e.g.*, [8, 9, 10]).

Our problem is peculiar not only due to the advection u, but also in the physical interpretation and observability of effects related to properties of formal solutions. Essentially, in the linear Schrödinger equation, different localized solutions to the linear problem do not mutually interact. In our fluid dynamical system, all these modes do mutually interact via nonlinearity and form a whole stationary flow, which may be almost everywhere intense for a high spatial density of localized modes. The role of nonlinearity for the the Schrödinger equation is addressed

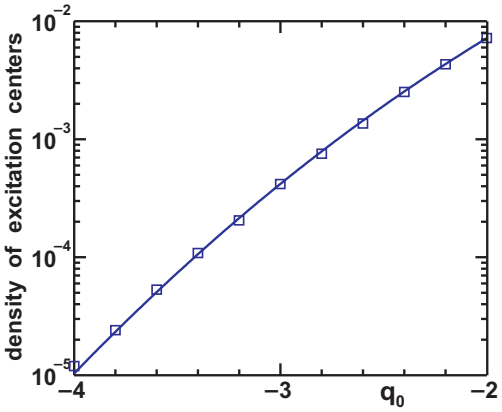

FIG. 2: Spatial density of centers of flow excitation in system (1) at $u = 0$. Squares: results of numerical simulation, solid line: dependence (4).

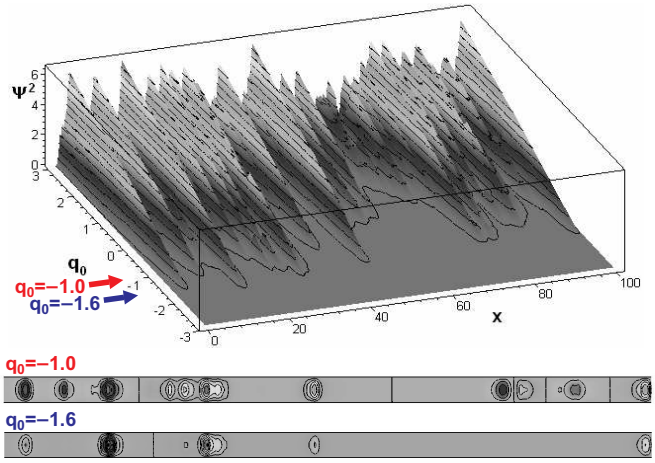

FIG. 3: The upper figure shows extinction of the excitation centers as q_0 decreases for a sample $\xi(x)$; the squared stream function amplitude $\psi^2(x, q_0)$ of the establishing pattern is plotted. The lower figures present flow stream lines for q_0 indicated in the plot (the scales of x and z are different). For $q_0 \lesssim -2$, no flows occur as the size of the domain presented becomes comparable to the mean distance between excitation centers (cf. Fig. 2).

in the literature (*e.g.*, [10, 17]) where it is reported to be able to lead to destruction of AL and other interesting effects. However, the physical meaning of the quantum wave function imposes strong limitations on the nonlinearity form (conservation of particles, *etc.*), whereas in a fluid dynamical system similar limitations are not applied. Therefore, the results of studies for nonlinear effects similar to [10, 17] may not (not always) be directly extended to the effects one faces in fluid dynamics.

As additionally follows from the above, localized flows can be observed for a low density of excited modes. This is the case of large negative deviation q_0 of the mean heat flux from the critical value. To make it clear let us consider a local mean value

$$q_l(x) \equiv \frac{1}{l}\int_{x-l/2}^{x+l/2} q(x_1)\,\mathrm{d}x_1\,.$$

When at the point x the value of $q_l(x)$ is positive for large enough l ("large enough l" means $l \sim 1$), one may expect a convective flow probably to arise in the vicinity of this point, while in the domain of negative q_l the convective flow is averagely damped. This criteria is rather qualitative and the specific value of l is not imposed by circumstances; for the sake of definiteness we choose $l = \pi$ [34] for representation of $q(x)$ in figures. For large negative q_0, positive values of q_l are of low probability and, therefore, the domains of an intense convective flow may be confidently expected to be sparse.

The last expectation is validated by numerical results [35] on the spatial density ν of the domains of flow excitation presented in Fig. 2. As q_l is a Gaussian random number with mean q_0 and variance $2/l$, the probability $P(q_l > 0)$ is the error function of $q_0\sqrt{l}/2$; for large negative q_0, $P(q_l > 0) \approx (-q_0)^{-1}(\pi l)^{-1/2}\exp(-q_0^2 l/4)$. Fortunately, the dependence

$$\nu_{\mathrm{app}} = 0.25\,P(q_{l=1.95} > 0) \qquad (4)$$

fairly fits the numerical results in Fig. 2. Note, the quantity ν makes sense only when excitation centers are separable, *i.e.*, the characteristic inter-center distance is large compared to the localization length. In Fig. 3 we show typical flow patterns and demonstrate extinction of the excitation centers as q_0 decreases for a sample $\xi(x)$. As excitation centers becomes sparse, separate localized flow patterns can be apparently discriminated and considered; Fig. 3 suggests $q_0 \lesssim -1.5$ to be the case.

III. LOCALIZATION EXPONENTS

A. Spatial Lyapunov exponents

Let us consider the stochastic system

$$\theta' = \psi, \quad \psi' = \phi, \quad \phi' = -[q_0 + \xi(x)]\psi - u\theta\,, \qquad (5)$$

which is equivalent to Eq. (3) with $S = 0$. One may treat the system (5) as a dynamic one with the spatial coordinate x instead of time and evaluate (spatial) Lyapunov exponents (LE) which yield eventually the localization exponents (*e.g.*, in review [10] the LE is employed as a localization exponent in order to estimate the localization length in classical AL).

The spectrum of LEs consist of three elements: $\gamma_1 \geq \gamma_2 \geq \gamma_3$. System (5) is statistically invariant under the transformation

$$(u, x, \theta, \psi, \phi) \to (-u, -x, \theta, -\psi, \phi)$$

[recall, $\xi(x)$ possesses spatially uniform and isotropic statistical properties and an even distribution]. Changing u to $-u$, this transformation simultaneously turns $\gamma_1(u)$,

$\gamma_2(u)$, $\gamma_3(u)$ into $-\gamma_1(u)$, $-\gamma_2(u)$, $-\gamma_3(u)$; after arrangement, one finds $-\gamma_3(u) \geq -\gamma_2(u) \geq -\gamma_1(u)$ which should be the spectrum $\gamma_1(-u) \geq \gamma_2(-u) \geq \gamma_3(-u)$. Therefore,

$$\gamma_1(q_0, u) = -\gamma_3(q_0, -u)\,, \tag{6}$$

$$\gamma_2(q_0, u) = -\gamma_2(q_0, -u)\,. \tag{7}$$

Additionally, the last relation means $\gamma_2(q_0, u = 0) = 0$. For $u = 0$ the system admits the homogeneous solution $\{\theta, \psi, \phi\} = \{1, 0, 0\}$, which corresponds to the very LE $\gamma_2 = 0$. As the divergence of the phase flow of system (5) is zero, $\gamma_1 + \gamma_2 + \gamma_3 = 0$; therefore,

$$\gamma_2(q_0, u) = -\gamma_1(q_0, u) + \gamma_1(q_0, -u)\,. \tag{8}$$

The properties (6)–(7) are demonstrated in Fig. 4a with the spectrum of LEs for $q_0 = -1$. Thus, due to (6) and (8), it is enough to calculate the greatest LE γ_1.

Fig. 4 shows the dependence of γ_1 (b) and γ_2 (c) on advection velocity u and mean supercriticality q_0. For any u, decrease of q_0 leads to growth of γ_1, *i.e.*, makes the localization more pronounced. For $q_0 < 0$, where localized flow patterns may occur, and non-large u, γ_1 decreases as u increases. In the following we will disclose the importance of the fact, that γ_2 is positive for positive u.

Let us now discuss relationships between the LEs evaluated and the solution properties. When, for $u = S = 0$, some flow is localized near x_0, in the distance from x_0,

$$\theta(x) \approx \begin{cases} \Theta_{2,-} + \Theta_1(x)\, e^{\gamma_1 (x - x_0)}, & x < x_0, \\ \Theta_{2,+} + \Theta_3(x)\, e^{\gamma_3 (x - x_0)}, & x > x_0, \end{cases}$$

where $\Theta_1(x)$ and $\Theta_3(x)$ are bounded functions (*i.e.*, neither decay nor grow averagely over large distances) determined by a specific realization of noise [36]. Considering the solution in between of two excitation domains near x_1 and $x_2 > x_1$, one can combine the above asymptotic laws for $x < x_0$ (assuming $x_0 = x_2$), *i.e.*, $\Theta_{2,-} + \Theta_1(x)\, e^{\gamma_1 (x - x_2)}$, and for $x > x_0$ (assuming $x_0 = x_1$), *i.e.*, $\Theta_{2,+} + \Theta_3(x)\, e^{\gamma_3 (x - x_1)}$, and obtain

$$\theta(x_1 < x < x_2) \approx \Theta_3(x) e^{\gamma_3 (x - x_1)} + \Theta_2 + \Theta_1(x) e^{\gamma_1 (x - x_2)}. \tag{9}$$

Here the amplitude of the corresponding stream function $\psi(x) \approx \Psi_3(x) e^{\gamma_3 (x - x_1)} + \Psi_1(x) e^{\gamma_1 (x - x_2)}$ [$\Psi_{1,3}(x)$ are bounded like $\Theta_{1,3}(x)$] is localized near x_1 and x_2 with the exponent γ_1 [$\gamma_3(q_0, u = 0) = -\gamma_1(q_0, u = 0)$]. Meanwhile, the temperature perturbation (9) is not localized because of constant Θ_2 which is generally different between different neighboring excitation regions.

For $u > 0$ (the case of $u < 0$ is similar and does not require special discussion), the shift of the temperature $\theta \to \theta + S/u$ eliminates the heat flux S. From the claim $S = 0$ for $u \neq 0$, it follows that in the domain of the flow damping, where $\psi \to 0$, the temperature perturbation θ tends to zero as well. Indeed, solution (9) takes the form

$$\theta(x_1 < x < x_2) \approx \Theta_3(x)\, e^{\gamma_3 (x - x_1)} + \Theta_2(x)\, e^{\gamma_2 (x - x_2)} + \Theta_1(x)\, e^{\gamma_1 (x - x_2)} \tag{10}$$

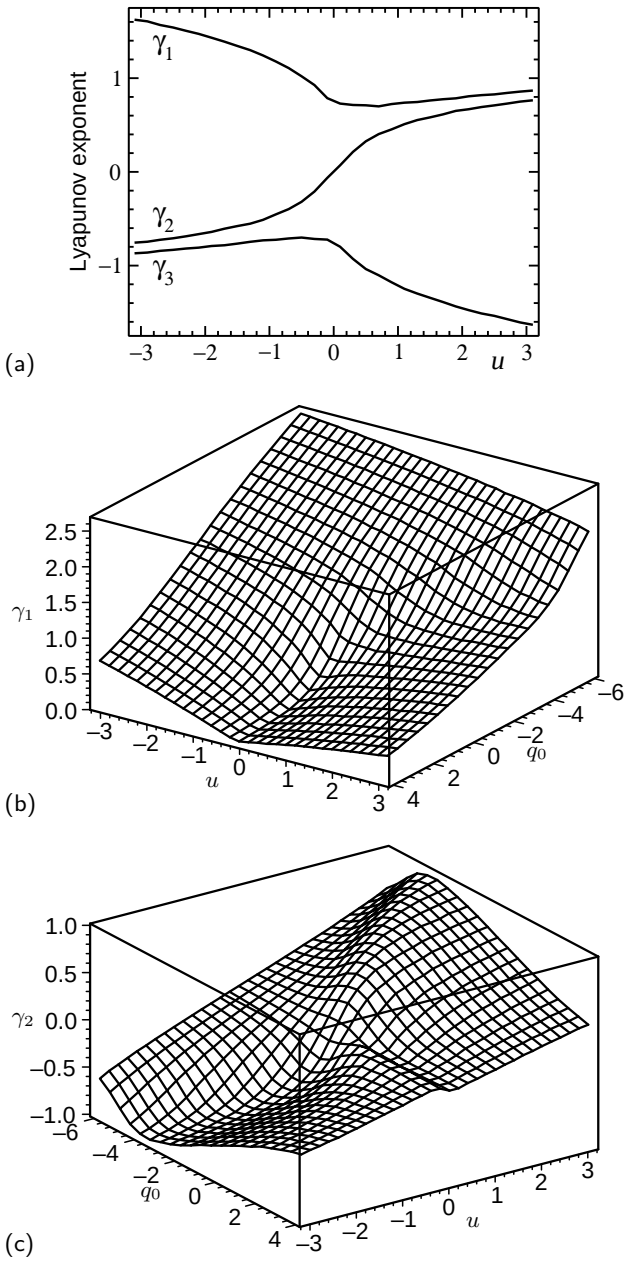

FIG. 4: Spectrum of Lyapunov exponents of system (5) is numerically evaluated by a direct simulation. Spectrum $\gamma_1 \geq \gamma_2 \geq \gamma_3$ at $q_0 = -1$ demonstrates the spectral properties in plot (a). The dependencies of γ_1 and γ_2 on u and q_0 are presented in plots (b) and (c), respectively.

[as $\gamma_2(q_0 < 0, u > 0) > 0$, the mode corresponding to γ_2 is localized near x_2], and, for $u \neq 0$, the contribution of the second term tends to 0 in the distance from excitation domains. Hence, in the presence of the advection the temperature perturbations are localized as well as the fluid currents. On the other hand, now the mode corresponding to γ_2 makes a nonzero contribution to the flow: $\psi(x) \approx \Psi_3(x) e^{\gamma_3 (x - x_1)} + \Psi_2(x) e^{\gamma_2 (x - x_2)} + \Psi_1(x) e^{\gamma_1 (x - x_2)}$.

As a result, for $\gamma_2 > 0$ ($u > 0$), the flow is localized down the advection stream (the right flank of the local-

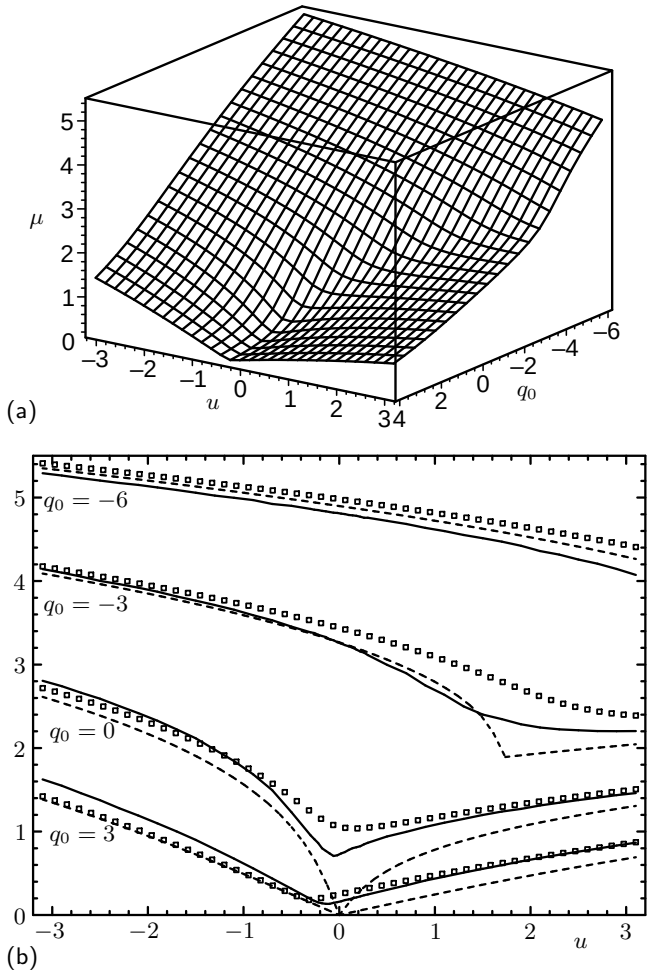

FIG. 5: (a): Greatest growth exponent μ of the mean-square temperature is plotted for system (5). (b): Exponent μ (squares) is compared to doubled greatest Lyapunov exponents $2\gamma_1$ of system (5) (solid line) and of the noiseless system (dashed line). Though for $q_0 < 0$ the trivial solution of the noiseless system is absolutely stable, the latter exponent formally calculated for system (5) with $\xi(x) = 0$ provides a rough approximation to the Lyapunov exponent of system (5) in the presence of disorder.

ized flow) with the exponent γ_3; $\gamma_- = |\gamma_3|$. On the left flank of the excitation domain, two modes appear:

$$\psi(x < x_2) \approx \Psi_2(x)\, e^{\gamma_2(x-x_2)} + \Psi_1(x)\, e^{\gamma_1(x-x_2)}. \quad (11)$$

For moderate u, $\Psi_1(x)$ are $\Psi_2(x)$ are comparable; hence, the mode $\Psi_1(x)e^{\gamma_1(x-x_2)}$ rapidly "disappears" against $\Psi_2(x)e^{\gamma_2(x-x_2)}$ as one moves away from x_2, and the upstream localization properties are determined by γ_2; $\gamma_+ = \gamma_2$. For $u = 0$, the function $\Psi_2(x) = 0$, and, for small u, $\Psi_2(x)$ remains small by continuity. In the last case the flow (11) considerably decays in the domain where the γ_1-mode remains dominating over the small γ_2-one, and this mode determines the upstream localization length; $\gamma_+ = \gamma_1$.

B. Growth exponents of mean-square values

For an analytical estimation of the greatest LE one may consider behavior of mean-square values of fields (see [3]; *e.g.*, in the paper [18], such an approach was utilized for approximate analytical calculation of the Lyapunov exponent for a stochastic system similar to system (5)). Specifically, we make use of the following particular result of [3], which is valid for a linear system of ordinary differential equations with noisy coefficients:

$$y_i' = L_{ij}\, y_j + \xi(x)\, \Gamma_{ij}\, y_j\,.$$

For normalized Gaussian δ-correlated noise $\xi(x)$ [$\langle \xi(x) \rangle = 0$, $\langle \xi(x+x')\xi(x) \rangle = 2\delta(x')$], the mean values $\langle y_i \rangle$ (averaged over noise realizations) obey the equation system

$$\langle y_i \rangle' = (\mathbf{L} + \mathbf{\Gamma}^2)_{ij} \langle y_j \rangle \quad (12)$$

(a simple rederivation of the particular result (12) can be found in [18]).

For $\vec{y} = \{\theta, \psi, \phi\}$, matrix $\mathbf{\Gamma}^2 = 0$, and noise does not manifest itself. This is due to the system symmetry and does not characterize behavior of a particular system under given realization of noise. In order to characterize this behavior, one have to consider behavior of mean-square values (cf. [3]). For $\vec{y} = \{\theta^2, \theta\psi, \theta\phi, \psi^2, \psi\phi, \phi^2\}$, Eqs. (5) yield

$$\begin{aligned}
y_1' &= 2y_2\,,\\
y_2' &= y_4 + y_3\,,\\
y_3' &= y_5 - [q_0 + \xi(x)]y_2 - uy_1\,,\\
y_4' &= 2y_5\,,\\
y_5' &= y_6 - [q_0 + \xi(x)]y_4 - uy_2\,,\\
y_6' &= -2[q_0 + \xi(x)]y_5 - 2uy_3\,.
\end{aligned}$$

Hence,

$$\mathbf{A} \equiv \mathbf{L} + \mathbf{\Gamma}^2 = \begin{bmatrix} 0 & 2 & 0 & 0 & 0 & 0 \\ 0 & 0 & 1 & 1 & 0 & 0 \\ -u & -q_0 & 0 & 0 & 1 & 0 \\ 0 & 0 & 0 & 0 & 2 & 0 \\ 0 & -u & 0 & -q_0 & 0 & 1 \\ 0 & 0 & -2u & 2 & -2q_0 & 0 \end{bmatrix}.$$

The growth exponent μ of mean-square values is the greatest real (as a mean-square value cannot oscillate) meaningful eigenvalue of matrix $\mathbf{A}$ [37]. Although the characteristic equation of matrix $\mathbf{A}$ is a 6-degree polynomial of μ, it is just a quadratic polynomial of u, and one can analytically find the surface of the greatest real $\mu(q_0, u)$, consisting of two sheets, in a parametric form:

$$u_{1,2} = \frac{7}{16}\mu^3 + \frac{1}{4}q_0\mu - \frac{1}{2} \pm \sqrt{\frac{81}{256}\mu^6 + \frac{27}{32}q_0\mu^4 - \frac{15}{16}\mu^3 + \frac{9}{16}q_0^2\mu^2 - \frac{3}{4}q_0\mu + \frac{1}{4}}\,. \quad (13)$$

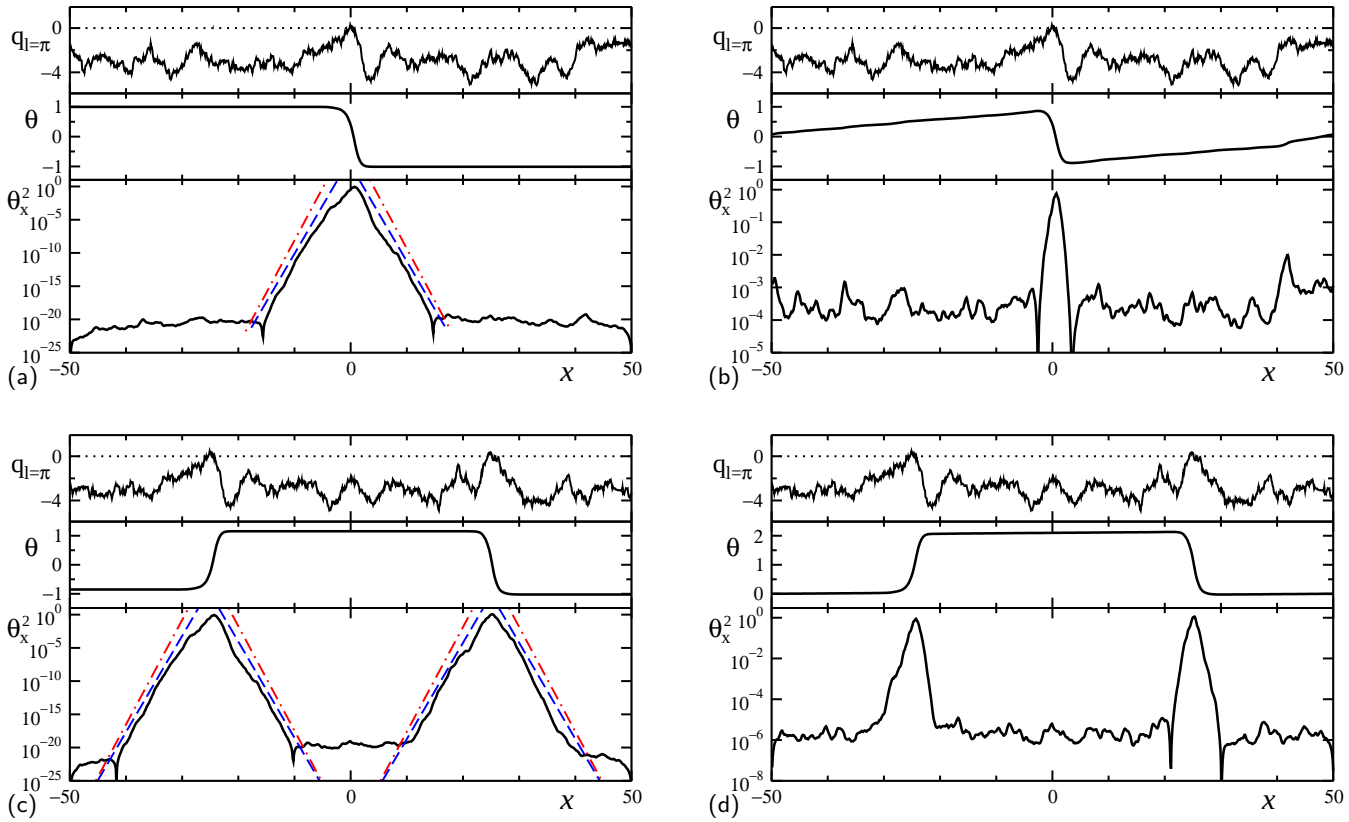

FIG. 6: Sample establishing time-independent solutions to Eq. (1) without advection for $q_0 = -3.1$ [realizations of $q(x)$ are represented by $q_{l=\pi}(x)$]. The lateral boundaries of the domain ($x = \pm 50$) are thermally-insulating impermeable (a,c), periodic (b), and isothermal impermeable (d). Dashed lines: the inclination corresponding to flow decay with the exponent $\gamma_1 = 1.67$, dashdot lines: decay with the exponent $\mu/2 = 1.81$.

These expressions make sense for $\mu > 0$, $q_0 \geq 2/3\mu - 3\mu^2/4 + \sqrt{2\mu/3}$. Fig. 5 presents this surface and demonstrates good agreement between $2\gamma_1$ and μ (which do not necessarily coincide by definition).

IV. NONLINEAR SOLUTIONS

In this section we
(i) underpin the findings of Sec. III with the results of numerical simulation for the nonlinear problem (1),
(ii) explore the role of lateral boundary conditions for a finite layer, and
(iii) discuss the consequences of the revealed fact that the flow patterns may be localized up the advection stream with exponent γ_2 which can be small.
Here our ultimate goal is to check and to show, that all the effects and localization peculiarities found with the linear system can be observed in the full nonlinear problem [thus, we validate the argument of Sec. II B, that the localization properties can be comprehensively studied by means of Eq. (3)].

Although the localization properties for the stationary linear equation (3) at $u = 0$ are well known, the behavior of the fluid dynamical system (1) in the absence of advection deserves particular attention due to above mentioned essential differences between this system and the Schrödinger equation for quantum systems.

In agreement with expectations (Sec. II B) on observability of localized flows for $q_0 < 0$, one can see samples of localized solutions for $u = 0$ in Fig. 6. With thermally insulating lateral boundaries (Fig. 6a), the localized flow is excited in the vicinity of the domain, where $q_{l=\pi}$ spontaneously takes positive values, and decays beyond the excitation domain (the background noise $\theta_x^2 \sim 10^{-25}$ is due to the limitation on numeric accuracy). Thermally insulating lateral boundary conditions for a finite observation domain are eventually "free" ones (no external impositions at the boundary) and thus correspond to a large (compared to the domain size) distance between excitation centers in an infinite layer. For $q_0 = -3.1$, this distance is indeed large, approximately $3 \cdot 10^3$ (see Fig. 2).

For periodic lateral boundary conditions (Fig. 6b), the finiteness of the distance between excitation centers effectively manifests itself (this distance is the system period). The system (3) with vanishing noise admits the trivial solution $\theta = q_0^{-1} S\, x$ which is related to a constant nonzero heat flux S. In the presence of noise, this mode turns into the time-independent solution $\theta' = q_0^{-1} S + \psi_1$,

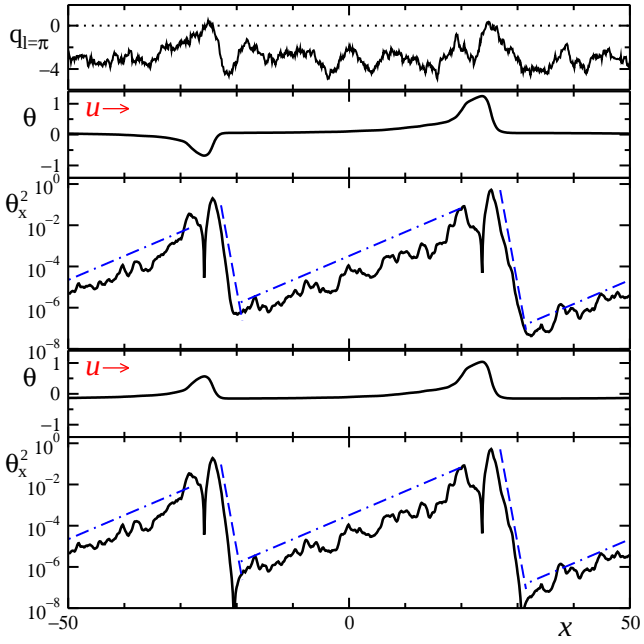

FIG. 7: Sample establishing time-independent solutions to Eq. (1) for $u = 0.3$, $q_0 = -3.0$ [$q(x)$ is represented by $q_{l=\pi}(x)$] and periodic lateral boundaries. Dashed lines: the inclination corresponding to flow decay with the exponent $\gamma_3 = 1.70$, dashdot lines: decay with the exponent $\gamma_2 = 0.134$. One also observes multistability (*i.e.*, coexistence of states stable to small perturbations) for each separate localized flow pattern; it can change its sign.

$\langle\psi_1\rangle = 0$, which for small S obeys the equation

$$\psi_1'' + [q_0 + \xi(x)]\psi_1 = -q_0^{-1} S\, \xi(x)\,,$$

[here $\langle\xi(x)\psi_1\rangle = 0$], *i.e.*, $\psi_1 \propto S$. In the presence of noise this solution dominates in the domain where flows are damped ($q_l < 0$). In the situation presented in Fig. 6b, $q_0^{-1}S = [\theta]/L_{\rm layer}$, where $[\theta] \approx 2$ is the temperature altitude imposed by the excited nonlinear flow, $L_{\rm layer} \approx 100$ is the system period (calculation domain size). The quantity $(S/q_0)^2 \approx 4\cdot 10^{-4}$ has exactly the order of magnitude corresponding to the background flow observed in the distance from the excitation center (Fig. 6b). This background flow distorts the localization and makes the localization exponents of the "tails" of the excited localized flow pattern hardly measurable. For a time-independent flow the heat flux S is constant over the layer; therefore the mean background flow $\langle\Psi\rangle \propto \langle\theta'\rangle = q_0^{-1}S$ remains constant over the layer even for a large number of excitation centers.

For thermally insulating lateral boundaries the heat flux S related to the background flow should decay to zero. Therefore with thermally insulating lateral boundaries the time-independent localized flow patterns occur without the background flow for an arbitrary number of excitation centers (Fig. 6c). In its turn, with isothermal lateral boundaries (specifically, maintained under constant temperature $\theta = 0$) the intensity of the background flow decreases as the layer extends. The reason is that, for practically separated localized flow patterns, there is multistability between solutions with different signs of the temperature jumps in domains of intense flows; hence, with a large number of excitation centers, the jumps can be mutually balanced, resulting in a small value of $q_0^{-1}S = L_{\rm layer}^{-1}\sum_j [\theta]_j$ (*e.g.*, in Fig. 6d the background flow is considerably smaller than in Fig.6b). Strictly spiking, for independent random $[\theta]_j$, the sum $\sum_j [\theta]_j \propto \sqrt{L_{\rm layer}}$, and, hence, $q_0^{-1}S \propto L_{\rm layer}^{-1/2}$.

Sample flows for $u \neq 0$ are shown in Fig. 7. In agreement with predictions of Sec. III A, the temperature is equal on the both sides of an intense flow domain, *i.e.*, not only flows are localized but also temperature perturbations. And, which is more noteworthy, even for quite small u when γ_2 is also small, the localization properties up the advection stream are determined by γ_2, but not by γ_1 which is valid for vanishing u (as explained in Sec. III A), *i.e.*, these properties may change drastically. For instance, in Fig. 7 for $u = 0.3$ the upstream localization length increases by factor 12 compared to the one in the absence of advection. The fact, that advection causes upstream delocalization but not downstream, is qualitatively similar to the situation with barchan sand dunes, windward flank of which is flat [19, 20].

Noteworthy, the advectionally increased localization length becomes comparable to the mean distance between the excitation centers (Fig. 2) for moderate negative q_0. In this way, weak advection may lead to the transition from a set of localized convective flow areas to an almost everywhere intense "global" flow, and, for instance, drastically enhance transport of a nearly indiffusive pollutant which is transferred rather convectively than by the molecular diffusion. Quantitative analysis of these effects is a separate and laborious physical problem and will be considered elsewhere (this problem has already been initiated in [21] but without an imposed advection).

V. ADVECTIONAL WASHING-OUT OF LOCALIZED CONVECTIVE FLOWS

A. Temporal evolution of the system

In the previous sections we discussed only time-independent states, whereas in the presence of a strong advection the establishing regimes can be expected to be time-dependent. Indeed, let us consider a positive spatially uniform $q(x) = const > 0$. In such a case a time-independent space-periodic pattern establishes without advection. Advection u turns this mode into a traveling wave [in the reference frame moving with velocity u the advectional term in Eq. (1) vanishes]. Inhomogeneities of $q(x)$ destroy the space shift symmetry of Eq. (1) and affect the traveling wave regime. In our noisy case, when the excitation domain is very narrow, the pattern confined between the damping regions is locked and frozen,

while for a broader excitation domain, a successor of this traveling wave may occur.

Before we could discuss results related to the temporal evolution of patterns for irregular $q(x)$, an important fact, which may seem to be counterintuitive at the first glance, should be addressed. In spite of disorder in $q(x)$ the temporal evolution of a certain solitary localized pattern is a deterministic process but not a stochastic one [38]. In order to support this fact, let us recall a situation comprehensively studied in the literature (*e.g.*, [22, 23]), the case of a null-dimensional system driven by a noisy time-dependent signal. In that case the temporal evolution of the system is a stochastic process. Nevertheless, for an ensemble of these systems driven by common noise the patterns in the phase space at a certain moment of time (so-called "snapshot attractors") either are smooth or have a fractal structure which is, however, proper to deterministic chaos but not to stochastic one, even though reference points of these patterns stochastically evolve in time. In this paper we deal with a situation which is mathematically similar to the recalled one up to the exchange of time and space. In the same fashion as, in the case of time-dependent spatially homogeneous noise, spatial patterns are regular, in the case of time-independent disorder in parameters, the temporal evolution is smooth and deterministic.

We do not construct a rigorous proof that the temporal evolution is smooth and deterministic in our case (for the recalled "twin" situation a comprehensive discussion of the regularity property of snapshot attractors is developed in a series of works [22]). Instead, a rough intuition for this fact can be provided with the problem of the linear stability of the trivial state. Without disorder the eigenvalue spectrum of this problem is bounded from above (infinitely fast growing modes are not possible). Disorder in $q(x)$ leads to a spreading of the spectrum. However, shifts of eigenvalues related to this spreading are finite [9], *i.e.*, the spectrum remains bounded from above. In the presence of disorder, eigenfunctions $g_\lambda(x)$ corresponding to eigenvalues λ become nonsmooth but remain finite. Thus, solution $\theta(x,t) = \sum_\lambda C_\lambda e^{\lambda t} g_\lambda(x)$ [C_λ are amplitudes] to the linear problem evolves in time deterministically in spite of irregularity of $g_\lambda(x)$. The results of numerical simulation for Eq. (1) as well show spatially irregular patterns to evolve regularly in time.

B. Scenarios of washing-out

The imposed longitudinal advection u leads not only to the upstream spreading of localized flows but also suppresses these flows. For an everywhere intense flow it is not obvious (without special study) whether the advection enhances or suppresses convection. Differently, with a localized flow pattern, the advection washes away the heat perturbations from the excitation domain and, in this way, suppresses convection. In the simplest case, as one increases the advection strength, the intensity of a convective flow decreases till it disappears via a pitchfork bifurcation (scenario I) where the trivial state becomes the only attractor. In scenario I, establishing flows are always time-independent. For some realizations of noise (quite often) the convective flow disappears via a Hopf bifurcation near the trivial state (scenario II; here the oscillatory mode is a successor of the traveling wave regime discussed above). Moreover, in scenario II, multistability and hysteresis transitions as u changes are observed (the Hopf bifurcation is only the last stage of this complex scenario).

Let us discuss complex scenario II in details for a sample realization of $q(x)$ shown in Fig. 10a and periodic boundary conditions. Fig. 8 presents the evolution of the establishing temperature altitude and stability properties of the establishing states and of the trivial one as u increases. First, let us note that close to point **P** the leading eigenvalue of the problem of the linear stability of the trivial state is small and turns complex (gray curves in Fig. 8c); therefore the system is close to a co-dimension 2 bifurcation where two real eigenvalues turn to zero, but this bifurcation differs from a Bogdanov–Takens one [24] due to the sign inversion symmetry ($\theta \to -\theta$) of our system. Such a situation (closeness to a Bogdanov–Takens bifurcation affected by the sign inversion symmetry of the fields) is wide spread in fluid dynamics and, *e.g.*, Knobloch and Proctor have encountered it for the problem of convection in an imposed vertical magnetic field [25]. As on some stages of the bifurcation scenario the central manifold of the system is 2D (cf. [25]), we project system trajectories onto the 2D plane $(\|x\theta\|, \|x^2\theta\|)$ (henceforth, the notation $\|...\| \equiv \int_{L_{\rm layer}} ... \,{\rm d}x$ stands for integration over the calculation domain) for presentation in Fig. 9 [these linear in θ integral quantifiers of the pattern $\theta(x)$ are the simplest independent ones].

In the absence of advection, only time-independent flows can establish. For small u, this is still valid by continuity (Fig. 9a). As advection becomes stronger, a pair of finite-amplitude oscillatory flows (Fig. 9b) appears at $u = u_{\rm T} \approx 0.754$ via a tangential bifurcation (point **T** in Fig. 8); the more intense periodic flow is locally stable (Fig. 9b, solid loop: stable limit cycle, dashed curve: saddle cycle). At $u_{\rm Sh} \approx 0.75956$ (**Sh** in Fig. 8b), the unstable manifold of the origin intersects the stable one and two homoclinic loops appear (Fig. 9c; Fig. 10d presents the temporal evolution of the homoclinic solution); the union of these loops is the former unstable cycle. Simultaneously with these repelling loops, the locally stable periodic (Figs. 9c,10c) and time-independent flows (Figs. 9c,10e) exist (the homoclinic loops belong to the boundary between the attraction basins of these stable flows). For stronger advection, $u_{\rm Sh} < u < u_{\rm H_{sub}}$, the homoclinic loops turn into a pair of unstable cycles (Fig. 9d) [39], which shrink as u increases and collapse onto the time-independent solutions making them unstable via a subcritical Hopf bifurcations at $u_{\rm H_{sub}} \approx 0.775$ (**$\mathbf{H_{sub}}$** in Fig. 8). For $u_{\rm H_{sub}} < u < u_{\rm H_{sup}}$, the only stable

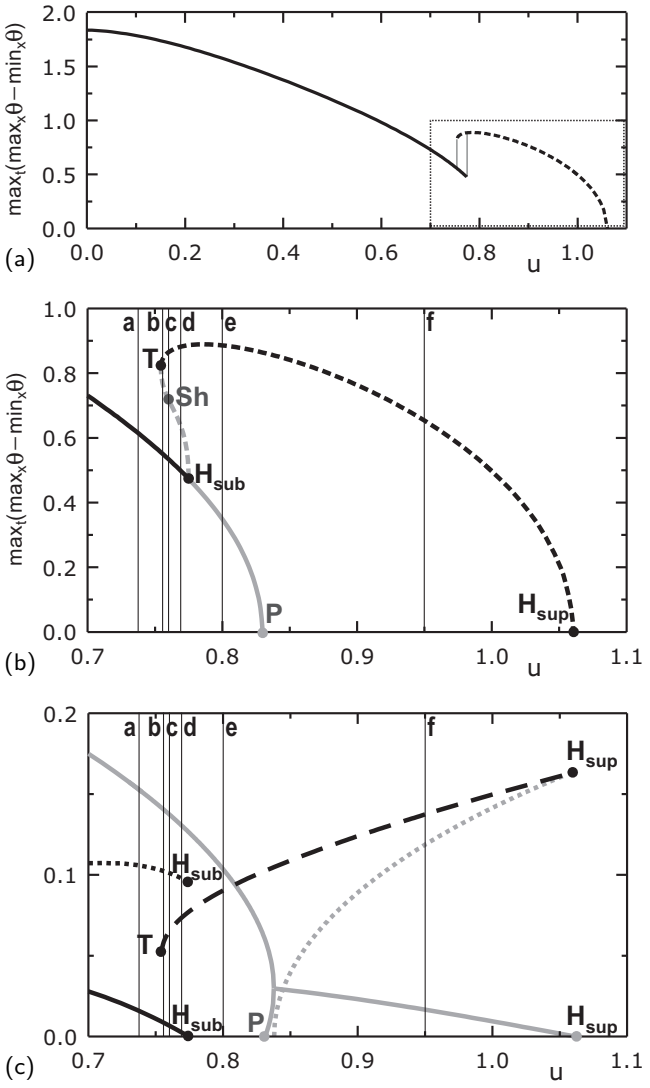

FIG. 8: Scenario of the washing-out of the localized convective flow in the system (1) is numerically calculated for $q(x)$ plotted in Fig. 10a. (a): the altitude of the temperature field $[\theta] \equiv \max\theta(x) - \min\theta(x)$ of the time-independent stable pattern (solid line) and the maximal value of the one for the stable oscillatory regime (dashed line). (b): zoom-in of the region marked by the rectangle in plot (a); gray lines present unstable regimes. (c): the black lines present the exponential decay rate (solid line) and the frequency (dotted line) of perturbations of the time-independent pattern and the frequency of the stable oscillatory flow (dashed line); the gray lines present the exponential growth rate (solid) and the frequency (dotted) of perturbations of the trivial state. For the values of u marked by vertical lines with letters in plots (b,c), projections of the phase portraits are shown in Fig. 9 under the corresponding letters.

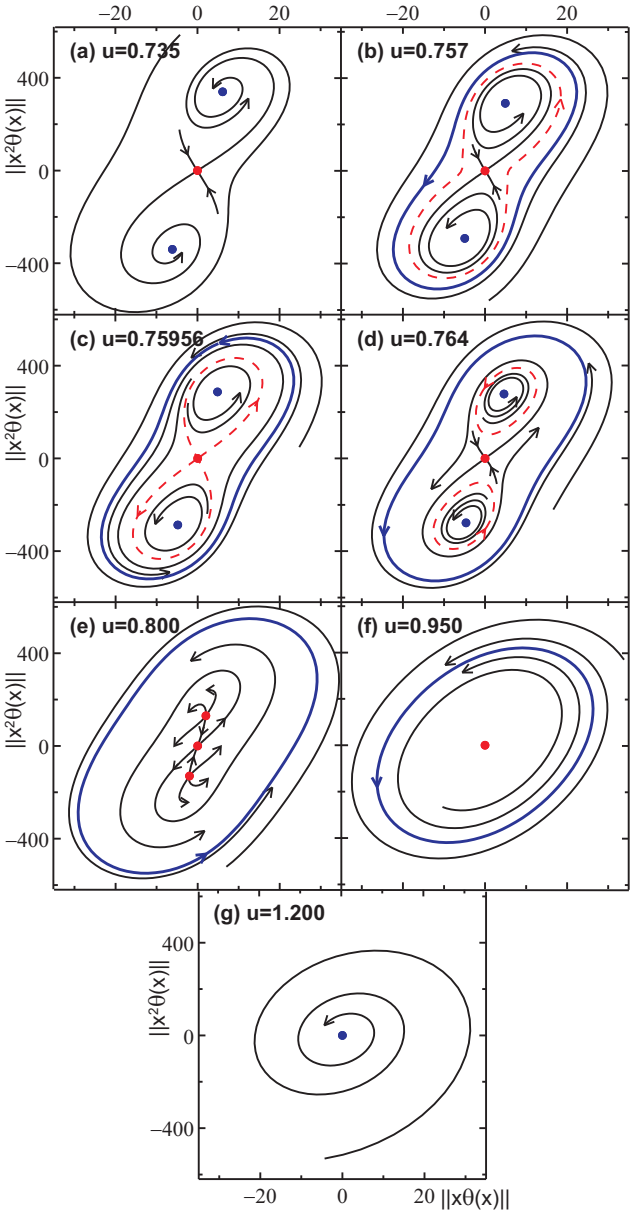

FIG. 9: (Color online) Projections of trajectories of the system (1) onto the plane $(\|x\theta\|, \|x^2\theta\|)$ are calculated for the values of u indicated in the plots and $q(x)$ presented in Fig. 10a.

regime is the oscillatory flow (Figs. 9e,f,10b). Within this range of u, at $u_{\rm P} \approx 0.832$, the unstable time-independent flows disappear via a pitchfork bifurcation near the trivial state (**P** in Fig. 8), turning it from a saddle into an unstable focus (Fig. 9f). For $u > u_{\rm P}$, increase of u leads to a shrinking of the limit cycle till the oscillatory flow diminishes to zero at $u_{\rm H_{sup}} \approx 1.062$ and disappears via a supercritical Hopf bifurcation (**$\mathbf{H_{sup}}$** in Fig. 8). For $u > u_{\rm H_{sup}}$, all flows decay (Fig. 9g). Remarkably, the vicinity of trivial state belongs to the attraction basin of the time-independent flows for $u < u_{\rm Sh}$ and to the one of the oscillatory flow for $u_{\rm Sh} < u < u_{\rm H_{sup}}$.

The scenario of the washing-out depends on the specific realization of noise; therefore no universal quantitative description may be developed. Nevertheless, one may roughly conclude that, for narrow excitation domains [*i.e.*, where $q_l(x)$ has a spontaneous uplift which is high but narrow], the system preferably follows sce-

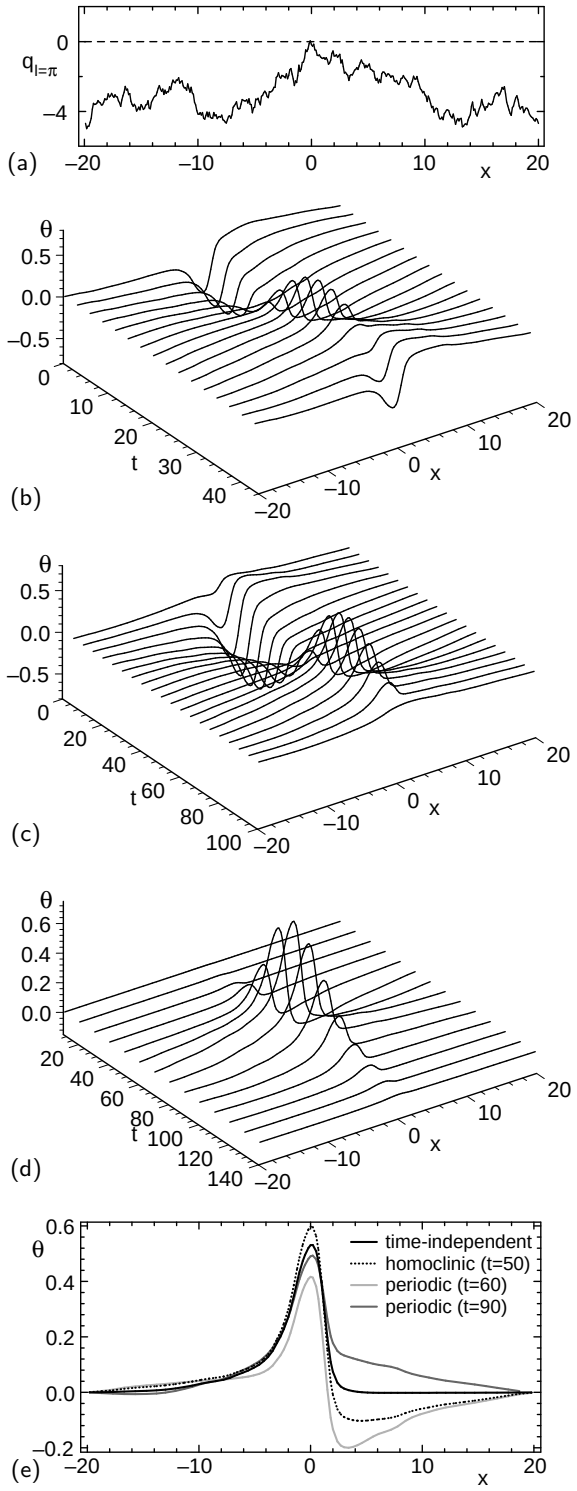

FIG. 10: Temporal evolution (b,c,d) of temperature field for sample $q(x)$ (a). (b): stable periodic solution at $u = 0.95$, (c,d): stable periodic solution and homoclinic one at $u_{\rm Sh} \approx 0.75956$, respectively, (e): stable time-independent state compared to homoclinic and two periodic patterns (two profiles are distant in time by a quarter-period) at $u_{\rm Sh}$ [for time-dependent states, time is the same as in (c,d)]. One sees the difference in the temporal evolution of these patterns to not come from their topological difference which is not much pronounced.

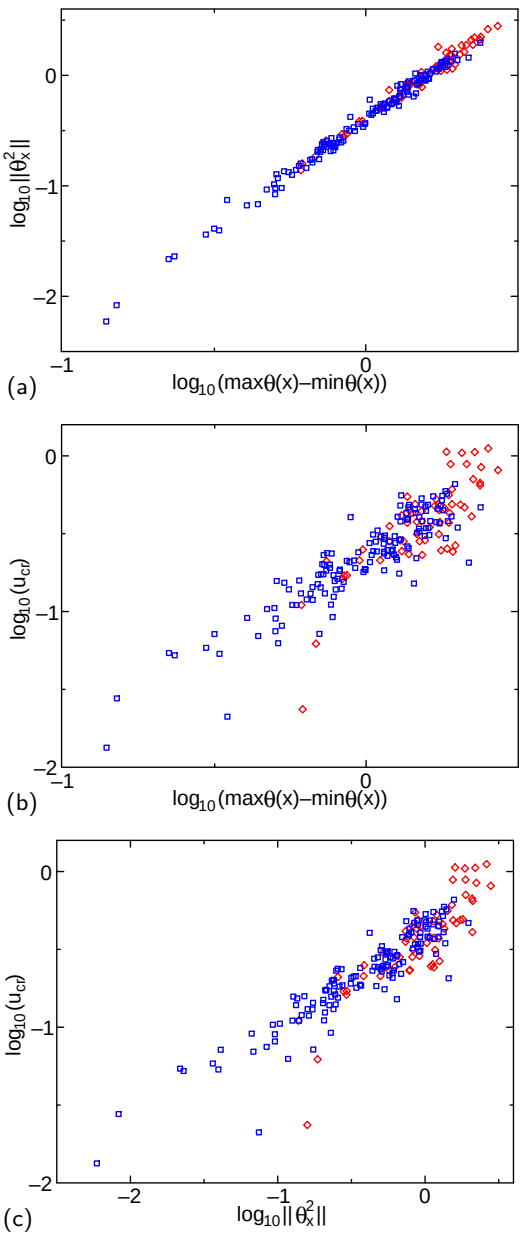

FIG. 11: (Color online) Integral characteristics of localized patterns at $q_0 = -3$, $u = 0$. (a): flow intensity $\|\theta_x^2\| \equiv \int_L \theta_x^2 {\rm d}x$ vs temperature altitude $[\theta]$; (b) and (c): critical advection strength $u_{\rm cr}$ vs $[\theta]$ and $\|\theta_x^2\|$, respectively. Blue squares: the convective flow disappears via a pitchfork bifurcation, red diamonds: via a Hopf one.

nario I, while, for broader ones, scenario II becomes more probable.

Rough correlations between different integral characteristics of localized patterns without advection and the critical advection strength $u_{\rm cr}$ (at $u_{\rm cr}$ the localized flow disappears; for scenario II, $u_{\rm cr} \equiv u_{\rm H_{sup}}$) can be observed for different realizations of noise (Fig. 11; [40]). One may note quite strong correlation between $[\theta]$ and $\|\theta_x^2\|$ in Fig. 11a, whereas correlations between critical ad-

vection strength $u_{\rm cr}$ and integral quantifiers of the flow in the absence of advection are not so well pronounced (Fig. 11b,c).

Additionally, Fig. 11 shows washing-out scenario II to be the most probable one for intense convective flows and very rare for weak ones. This fact is in agreement with the results on the problem of the linear stability of the trivial state for sample $q(x)$. The dependence of the leading eigenvalue of this problem on u (gray lines in Fig. 8c) possesses a similar shape for any realization of $q(x)$, but point **P** where the eigenvalue turns complex can be either above or below the u-axis. In the former case, scenario II occurs, whereas, in the latter one, the localized flow disappears before the time-dependent regimes can be excited, the system follows scenario I. On the other hand, the less intense flows (without advection) are proper to the lower positions of the discussed dependence for which the case of **P** lying below the u-axis, *i.e.*, scenario I, is more probable, and, *vice versa*, the more intense flows the higher probability of scenario II.

VI. CONCLUSION

We have studied the localization phenomenon in the problem of thermal convection in a thin horizontal layer subject to random spatial inhomogeneity, including the effect of an imposed longitudinal advection. The study relies on the equations relevant to a broad variety of fluid dynamical systems [11, 14, 15, 16] and some other active media where pattern formation occurs; for instance, the Kuramoto–Sivashinsky equation (*e.g.*, [26] and refs. therein for examples of physical systems) has the same linear part as Eq. (1) with $u = 0$. Moreover, the basic laws in physics are conservation ones, what quite often remains in the final equations having the form $\partial_t[\text{quantity}] + \nabla \cdot [\text{flux of quantity}] = 0$ (*e.g.*, in [27] the equation for the Eckhaus instability mode in a system relevant, for instance, to binary convection at small Lewis number [28] preserves such a form). With such conservation laws either for systems with the sign inversion symmetry of the fields, which is quite typical in physics, or for description of spatial modulation of an oscillatory mode, the Kuramoto–Sivashinsky equation should be modified exactly to Eq. (1). Noteworthy, for thermal convection in a porous layer [11], the frozen parametric disorder $\xi(x)$ may be due to random inhomogeneities of the porous matrix (which are inevitable in reality), while the mean supercriticality q_0 may be controlled in experiments.

Summarizing, localized nonlinear flow patterns have been observed below the instability threshold of the system without disorder, and the dependence of the spatial density of the localized flow patterns on the mean departure q_0 from this threshold has been found numerically [Fig. 2, approximate expression (4)]. The up- and downstream localization exponents have been evaluated numerically (Fig. 4) and estimated analytically [Eq. (13)]. In particular, the advection has been found to result in the localization of the temperature perturbation in addition to the convective flow (the former is not localized in the absence of advection). In agreement with theoretical predictions, numeric simulation for the nonlinear equation has exhibited a crucial effect of the advection on the upstream localization properties; the localization length can increase by one order of magnitude for small finite u. Via the upstream delocalization, weak advection may lead to the transition from a set of localized flow patterns to an almost everywhere intense "global" flow, and, *e.g.*, essentially enhance transport of a nearly indiffusive pollutant (without advection the problem has been addressed in [21] where a crucial role of the localized flow patterns for such a transport has been revealed and discussed).

Moderate and strong advection washes out localized flows. This washing-out phenomenon has been studied for many sample realizations of noise, revealing two possible scenarios: via a pitchfork bifurcation (I) and via a sequence of bifurcations finishing with a Hopf one (II). Scenario II has been discussed in details for a sample noise realization; multistability and hysteresis transitions were observed.

Acknowledgments

The authors are thankful to Prof. Arkady Pikovsky, Dr. Michael Zaks, Prof. Dmitry Lyubimov, and Dr. Sergey Shklyaev for interesting and seminal discussions and comments in the course of the research. The authors acknowledge the Foundation "Perm Hydrodynamics," the BRHE–program (CRDF Grant no. Y5–P–09–01 and MESRF Grant no. 2.2.2.3.16038), and the VW–Stiftung for financial support.

[1] P. W. Anderson, Phys. Rev. **109**, 1492 (1958).
[2] J. D. Maynard, Rev. Mod. Phys. **73**, 401 (2001).
[3] V. I. Klyatskin, *Dynamics of Stochastic Systems* (Elsevier, Amsterdam, 2005).
[Originally in Russian: V. I. Klyatskin, *Statistical description of dynamic systems with fluctuating parameters* (Nauka, Moscow, 1975)]
[4] D. R. Grempel, Sh. Fishman, and R. E. Prange, Phys. Rev. Lett. **49**, 833 (1982).
[5] E. Borgonov and D. L. Shepelyansky Physica D **109**, 24 (1997).
[6] J. Bourgain and W.-M. Wang, Commun. Math. Phys. **248**, 429 (2004).
[7] M. Hammele, S. Schuler, and W. Zimmermann, Physica D **218**, 139 (2006).
[8] J. Fröhlich and T. Spencer, Phys. Rep. **103**, 9 (1984).

[9] I. M. Lifshitz, S. A. Gredeskul, and L. A. Pastur *Introduction to the Theory of Disordered Systems* (Wiley, New York, 1988).

[10] S. A. Gredeskul and Yu. S. Kivshar, Phys. Rep. **216**, 1 (1992).

[11] D. S. Goldobin and E. V. Shklyaeva, *Large-Scale Thermal Convection in a Horizontal Porous Layer*, Phys. Rev. E (*submitted*, 2008). [preview: arXiv:0804.2825]

[12] E. M. Sparrow, R. J. Goldstein, and V. K. Jonsson, J. Fluid Mech. **18**, 513 (1964).

[13] *Transport Phenomena in Porous Media*, edited by D. B. Ingham and I. Pop (Pergamon, Oxford, 1998).

[14] E. Knobloch, Physica D **41**, 450 (1990).

[15] L. Shtilman and G. Sivashinsky, Physica D **52**, 477 (1991).

[16] S. N. Aristov and P. G. Frick, Fluid Dyn. **24**, 690 (1989).

[17] A. S. Pikovsky and D. L. Shepelyansky, Phys. Rev. Lett. **100**, 094101 (2008).

[18] R. Zillmer and A. Pikovsky, Phys. Rev. E **72**, 056108 (2005).

[19] H. J. Herrmann and G. Sauermann, Physica A **283**, 24 (2000).

[20] G. Sauermann *et al.*, Geomorphology **36**, 47 (2000).

[21] D. S. Goldobin and E. V. Shklyaeva, *Diffusion of a passive scalar by convective flows under parametric disorder*, J. Stat. Mech. (*preprint*, 2008). [preview: arXiv:0805.1518]

[22] L. Yu, E. Ott, and Q. Chen, Phys. Rev. Lett. **65**, 2935 (1990); Physica D **53**, 102 (1991).

[23] D. S. Goldobin and A. Pikovsky, Phys. Rev. E **71**, 045201(R) (2005).

[24] Yu. A. Kuznetsov, *Elements of Applied Bifurcation Theory. Series: Applied Mathematical Sciences* Vol. 112, 3rd ed. (Springer, New York, 2004).

[25] E. Knobloch and M. R. E. Proctor, J. Fluid. Mech. **108**, 291 (1981).

[26] D. Michelson, Physica D **19**, 89 (1986).

[27] R. B. Hoyle, Phys. Rev. E **58**, 7315 (1998).

[28] W. Schöpf and W. Zimmermann, Europhys. Lett. **8**, 41 (1989); Phys. Rev. E **47**, 1739 (1993).

[29] D. S. Goldobin and D. V. Lyubimov, JETP **104**, 830 (2007).

[30] L. P. Shilnikov, Soviet Math. Dokl. **7**, 1155 (1966).

[31] Remarkably, for a large departure from the instability threshold the large-scale approximation can be utilized as well, and the equations (in [29] they have been derived for an even more general problem) are simpler than the ones relevant near the threshold. But those equations admit discontinuities of spatial derivatives of the temperature field, and these discontinuities cannot be studied within the framework of the large-scale approximation.

[32] Performing the rescaling, one should keep in mind, that the statistical effect of a delta-correlated noise is determined by the integral of its correlation function which is influenced by coordinate stretching. In details, under the rescaling $q = \mathcal{Q}\tilde{q}$ (and thus $\xi = \mathcal{Q}\tilde{\xi}$), $x = \mathcal{X}\tilde{x}$, and $t = \mathcal{T}\tilde{t}$, one finds $\langle \xi(x')\,\xi(x'+x)\rangle = 2D\,\delta(x) = 2D\,\mathcal{X}^{-1}\delta(\tilde{x}) = \mathcal{Q}^2\langle\tilde{\xi}(\tilde{x}')\,\tilde{\xi}(\tilde{x}'+\tilde{x})\rangle$. In order to obtain a normalized noise, *i.e.*, $\langle\tilde{\xi}(\tilde{x}')\,\tilde{\xi}(\tilde{x}'+\tilde{x})\rangle = 2\delta(\tilde{x})$, one should take $\mathcal{Q}^2 = D/\mathcal{X}$; to preserve Eq. (1) unchanged, one has to claim $\mathcal{T} = \mathcal{X}^4$ and $\mathcal{Q} = \mathcal{X}^{-2}$. These conditions yield $\mathcal{X} = D^{-1/3}$, $\mathcal{T} = D^{-4/3}$, and $\mathcal{Q} = D^{2/3}$.

[33] In order to proof this property of $\vec{v}$, let us consider the path Γ on the (x,z)-plane, which connects the point $\mathbf{\Gamma_1}$ to the point $\mathbf{\Gamma_2}$ on the lower and upper boundaries of the layer, respectively. The gross flux through this path is $J = \int_\Gamma \vec{v}\cdot\vec{n}\,\mathrm{d}l$, where $\vec{n}$ is orthogonal to Γ and directed into the same region as the gross flux, l is the length along Γ. Then $J = \int_\Gamma \left(v^x\frac{\mathrm{d}z}{\mathrm{d}l} + v^z\left(-\frac{\mathrm{d}x}{\mathrm{d}l}\right)\right)\mathrm{d}l = \int_\Gamma\left(\frac{\partial\Psi}{\partial z}\frac{\mathrm{d}z}{\mathrm{d}l} + \frac{\partial\Psi}{\partial x}\frac{\mathrm{d}x}{\mathrm{d}l}\right)\mathrm{d}l = \int_\Gamma\frac{\mathrm{d}\Psi}{\mathrm{d}l}\mathrm{d}l = \Psi(\mathbf{\Gamma_2}) - \Psi(\mathbf{\Gamma_1}) = 0$ because $\Psi = 0$ on the layer boundary [cf. Eq. (2)].

[34] The reason for such a choice is the fact, that in the noiseless case with all the coefficients equal 1 the fundamental mode is $\sin x$; for this mode the smallest space domain is of length π.

[35] All the numerical simulations for Eq. (1) are performed by means of the finite difference method (the first x-derivatives are central; the noiseless x-derivatives have accuracy $\mathrm{d}x^2$; the time step $\mathrm{d}t = \mathrm{d}x^4/11$; the noise $\xi(x)$ is generated in the middle between the mesh nodes). The space step $\mathrm{d}x = 0.1$ appears to be enough small for calculations what is ensured (i) by the results in Figs. 6,7 where the localization properties of calculated patterns are in agreement with the independent and much more accurate simulation for null-dimensional system (5) and (ii) by the fact, that statistical properties do not change when step $\mathrm{d}x$ is halved. This is due to the fact, that though a δ-correlated noise reduces the strong order of accuracy of numerical schemes, the weak order, that determines accuracy for statistical properties, is generally higher than the strong one.

[36] In order to write down these expressions on the both sides of point x_0, we take (in a general form) superpositions of all the eigenmodes corresponding to LEs $\gamma_1 > 0$, $\gamma_2 = 0$ (with spatially homogeneous eigenmodes $\Theta_{2,\pm}$), and $\gamma_3 < 0$ and exclude the ones that infinitely growth as we move away from x_0.

[37] A formal eigenvector is meaningful, when it meets the conditions $\langle\theta^2\rangle \geq 0$, $\langle\psi^2\rangle \geq 0$, $\langle\phi^2\rangle \geq 0$, $\langle\theta^2\rangle\langle\psi^2\rangle \geq \langle\theta\psi\rangle^2$, $\langle\theta^2\rangle\langle\phi^2\rangle \geq \langle\theta\phi\rangle^2$, and $\langle\psi^2\rangle\langle\phi^2\rangle \geq \langle\psi\phi\rangle^2$.

[38] In the case of inappropriate initial conditions, the first infinitesimally small period of evolution should be excluded (like for the conventional heat conduction equation where inconsistencies in boundary and initial conditions are known to decay infinitely fast).

[39] This bifurcation of homoclinic trajectories differs a bit from general ones described by the Shil'nikov's theorem [24, 30] due to the symmetry $\theta \to -\theta$.

[40] A precise and comprehensive investigation of the statistics on the prevalence of these scenarios and their peculiarities for different values of parameters is beyond the scope of the present paper